

Gravity-inferred crustal thickness of Greenland

Alexander Braun ^{a,*}, Hyung Rae Kim ^b, Beata Csatho ^c, Ralph R.B. von Frese ^d

^a *Department of Geomatics Engineering, Schulich School of Engineering, University of Calgary,
2500 University Dr. NW, Calgary, Canada AB T2N1N4*

^b *GEST/UMBC at Code 698, Planetary Geodynamics Lab, NASA/GSFC, Greenbelt, MD 20771, USA*

^c *Department of Geology, University at Buffalo, SUNY, Buffalo, NY 14260-3050, USA*

^d *School of Earth Sciences, The Ohio State University, 275 Mendenhall Laboratory, 125 South Oval Mall, Columbus, OH 43210-1308, USA*

Received 28 August 2006; received in revised form 22 June 2007; accepted 10 July 2007

Available online 3 August 2007

Editor: C.P. Jaupart

Abstract

Greenland's crust contains clues for understanding the dynamics of the Earth's second largest ice-sheet, as well as the Iceland hotspot over the past 100 Ma. However, our knowledge of the sub-ice crust is very limited due to the paucity of outcrops and seismic observations, particularly in central Greenland. In order to augment these sparse constraints, we modeled terrain and airborne free-air gravity data which provide estimates for Moho and related crustal thickness. These estimates were obtained from the inversion of isostatically corrected terrain effects where the computed gravity effects of the terrain's rock, water, and ice components were subtracted from the terrain-correlated free-air anomalies. The terrain-correlated free-air components were estimated from the correlation spectrum between the free-air anomalies and the terrain's gravity effects which are assumed to reflect isostatic disturbances of the crustal terrain. The results indicated an average crustal thickness of about 37 km for Greenland, with greater values by 5–10 km, in the southern Greenland Archean blocks and Caledonian Foldbelt, and comparably lower values in northern Greenland. The thinner crustal thickness estimates in the north are strongly correlated with the faster basal melt regions of the ice sheet and glaciers. The crustal thickness map provides constraints for an improved interpretation of the Iceland hotspot track in northern Greenland at about 100–70 Ma.

© 2007 Elsevier B.V. All rights reserved.

Keywords: Greenland; gravity; Moho; crustal thickness; generalized isostatic analysis; ice sheet; basal melt; Iceland hotspot

1. Introduction

The second largest ice sheet on Earth covers Greenland with a maximum ice thickness of about 3400 m (Alley et al., 1995). Its water equivalent would raise global sea level by about 7 m (Thomas et al., 2001). The glacial cycles of the Greenland ice sheet contribute to

global sea level change and are therefore strongly related to climate change. In order to assess and quantify these highly dynamic systems, new insights on atmospheric forcing (e.g. Bromwich et al., 1999), crustal deformation (Wahr et al., 2001), the thermal state of the crust at the base of the ice sheet, and other boundary conditions (Bamber and Payne, 2004) are required. In this study, we investigate Greenland's crust for thickness and isostatic constraints on crustal dynamics, heat flow patterns, and basal melting.

* Corresponding author. Tel.: +1 403 2204702; fax: +1 403 2841980.
E-mail address: braun@ucalgary.ca (A. Braun).

The crustal properties and evolution of Greenland are poorly known because ice at an average thickness of about 1.6 km covers roughly 80% of its land surface. Direct geological evidence of the crust is essentially restricted to outcrops along the ice-free coastal margins. Extrapolations of the coastal geology into the interior have established the major tectonic elements (Henriksen et al., 2000; Geological Survey of Denmark and Greenland, 2007), however the boundaries are not well defined, especially in northern and central Greenland. Thus, we must rely extensively on geophysical observations and modeling to uncover the crustal properties and processes of Greenland.

Geophysical surveying over the ice sheet has primarily employed airborne platforms to measure magnetic and gravity anomalies and ice probing radar soundings (Brozena, 1995; Korenaga et al., 2001; Forsberg and Kenyon, 2003). Additional ground penetrating radar data from both airborne and ground surveys have improved the mapping of Greenland's bedrock topography (Bamber et al., 2001; Layberry and Bamber, 2001). Seismic experiments on the ice sheet were also completed recently as part of the Greenland Lithosphere Analyzed Teleseismically on the Ice Sheet (GLATIS) project (Dahl-Jensen et al., 2003b). The distribution of seismic observations in Greenland is generally quite limited, therefore we primarily rely on magnetic and gravity anomaly observations for insights on the sub-ice geological features (Brozena, 1995; Korenaga et al., 2001; Forsberg and Kenyon, 2003).

Observed gravity anomalies reflect the horizontal density changes within both the crust and the mantle. Over the ice sheet, gravity anomalies can map the crustal topography, as well as compositional, structural, thermal, and other density variations of the crust and mantle. Within the lithosphere, the largest density contrasts occur between the crust and overlying air ($\Delta\rho \approx 2700 \text{ kg/m}^3$), ice ($\Delta\rho \approx 1800 \text{ kg/m}^3$), and water/ice ($\Delta\rho \approx 1700 \text{ kg/m}^3$) cover, whereas the second largest contrasts result between the crust and underlying mantle ($\Delta\rho \approx -400 \text{ kg/m}^3$).

At altitudes that are large compared to the relief of the crustal terrain, the gravity effects from these density contrasts are dominant, but tend to off-set each other due to crustal isostasy. However, where the crust is not in isostatic equilibrium, free-air gravity anomalies arise that strongly correlate with the gravity effects of the disturbed terrain (von Frese et al., 1999; Roman, 1999; Leftwich et al., 2005). To estimate these terrain-correlated free-air anomalies, the correlation spectrum (von Frese et al., 1997) can be used between the computed gravity effects of the terrain and the free-air gravity

anomaly observations (von Frese et al., 1999; Roman, 1999; Leftwich et al., 2005).

By subtracting the terrain's gravity effects from the terrain-correlated free-air anomalies, we estimate isostatically corrected terrain effects. At sufficiently high altitudes, these anomalies essentially reflect the effects of density contrasts defined by the Moho that seismic and other non-gravity methods image. Thus, the gravity Moho estimates from the inversion of these anomalies may be directly compared to and constrained by the available seismic Moho estimates (Dahl-Jensen et al., 2003b).

This generalized isostatic analysis is independent of any geographical projection and invokes no specific isostatic model for estimating or interpreting isostatic anomalies. It yields Moho estimates modeled for the gravity effects of the major density contrasts of the lithosphere constrained only by available terrain models and seismic Moho observations. The resultant gravity Moho estimates, however, are clearly not unique and can be interpreted for crustal flexure, elastic thickness, and other isostatic models of the lithosphere.

Generalized isostatic analysis fully accounts for the independent observations of the free-air gravity and the terrain data with minimum assumptions regarding the isostatic state of the lithosphere. However, the results are subject to several sources of error. For example, even though isostatically disturbed terrain always produces terrain-correlated free-air anomalies, not all of these anomalies necessarily reflect disturbed crustal terrain. These misclassification errors, as well as any errors in the terrain elevations, and densities assumed for the terrain and across the crust–mantle interface introduce errors in the Moho estimates.

The gravity effects of these errors, significantly attenuate with altitude because they commonly involve density contrasts at lower spatial scales and magnitudes relative to the major lithospheric density contrasts. For example, a 0.5° bathymetric error of $\pm 500 \text{ m}$ below sea level produces a sea level effect that is reduced by roughly 60% at 20-km altitude, whereas the same error over 5° results in a reduction of only 9% at this altitude (Leftwich et al., 2005). Furthermore, for terrain rock density errors, the amplitudes of the related gravity effects are diminished by more than an order of magnitude relative to the effects of the major lithospheric density contrasts. Hence, an analysis at 20-km altitude performed herein reduces terrain gravity noise relative to the regional signal of the terrain in the free-air anomalies.

The generalized analysis was developed and validated in crustal studies of the Antarctic (von Frese et al.,

1999), East Asia (von Frese et al., 1998), and the North Atlantic (Leftwich et al., 2005) where the gravity Moho estimates were found to be well within 10% of the available seismic estimates. It was also implemented for crustal studies of Venus (Leftwich et al., 1999), the Moon (Potts and von Frese, 2003a,b) and its Mare Orientale Basin (von Frese et al., 1997), and Mars (Potts et al., 2004). In a more local application, the analysis provided insight on the crustal properties and intraplate seismicity of Ohio (Kim et al., 2000).

For Greenland, we implement generalized isostatic analysis on terrain and airborne free-air gravity data sets for enhanced models of the Moho and related crustal thickness variations. These results yield new boundary conditions for glaciological and climate modeling, understanding the glacial and tectonic effects of crustal dynamics, and the thermal and mass flow dynamics of the Mid- Atlantic Ridge and Iceland hotspot. In addition, the crustal thickness variations define thermal conductivity contrasts and related surface heat flow

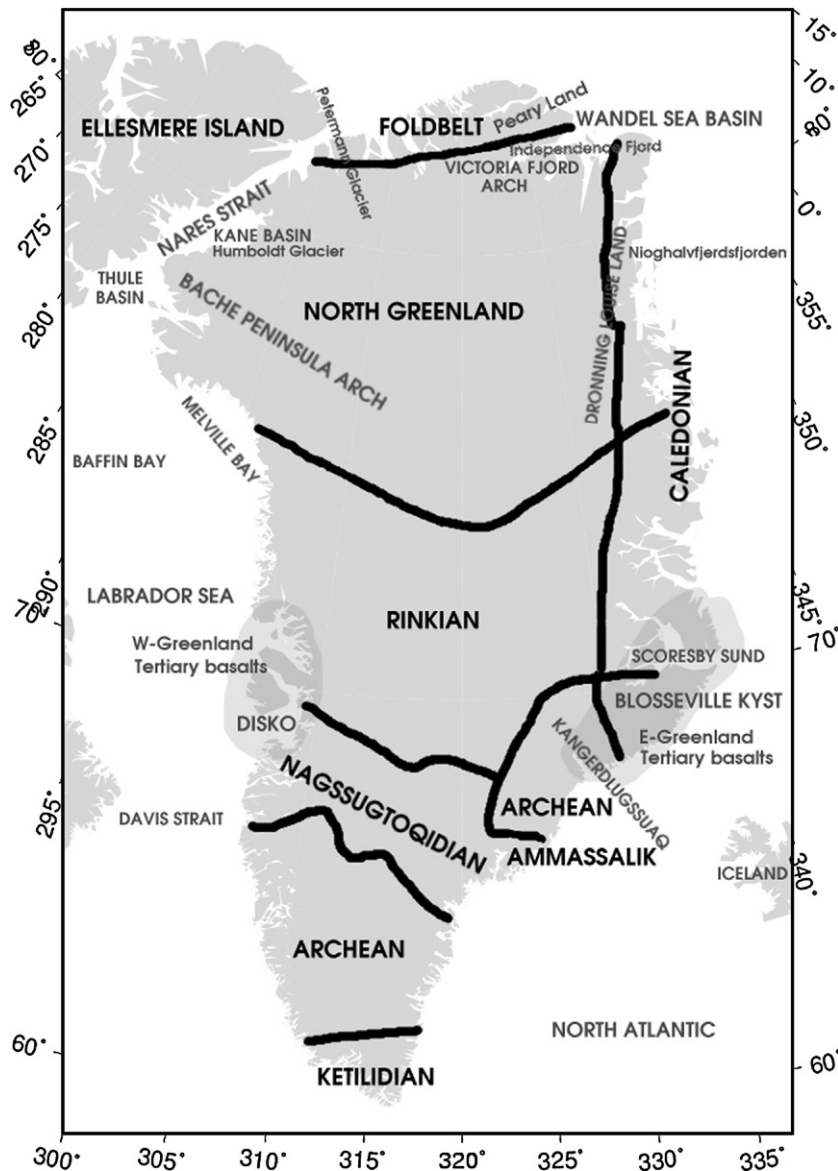


Fig. 1. Major tectonic and geographic features of Greenland and their respective boundaries. Map based on (Henriksen et al., 2000; Geological Survey of Denmark and Greenland, 2007) and (Brozena, 1995). Shaded areas in West-Greenland and East-Greenland denote the approximate location of tertiary basalts.

variations that affect basal melting and other glaciological processes.

In the following sections, we review the available geological and geophysical data and also investigate the details of estimating Greenland's Moho and related crustal thickness variations. The implications of these results on the crustal dynamics, heat flow patterns, and glacial dynamics of Greenland are also considered.

2. Tectonic setting

This section describes the tectonic setting of Greenland and the surrounding tectonic units and processes responsible for the present state of Greenland's crust and lithosphere. The tectonic situation is discussed together with the Iceland hotspot track and plate reconstructions.

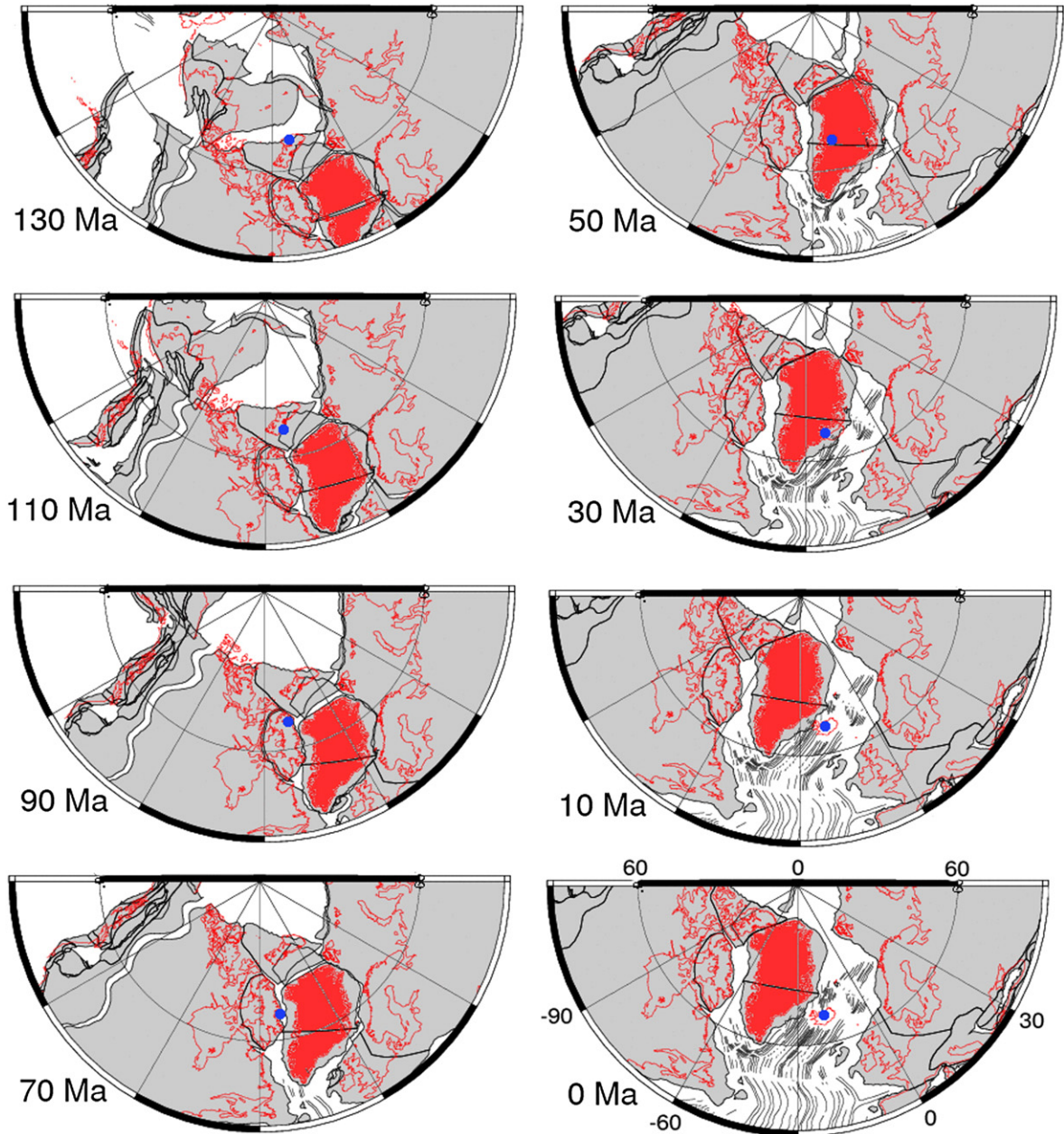


Fig. 2. Plate reconstruction based on a fixed hotspot frame and data from Müller et al. (1993). The blue dot marks the location of the Iceland hotspot. The figures were created using the ODSN Plate Tectonic Reconstruction Service (Hay et al., 1999) (For interpretation of the references to colour in this figure legend, the reader is referred to the web version of this article.).

2.1. Major tectonic units

A recent description of the geological map of Greenland by Henriksen et al. (2000), Geological Survey of Denmark and Greenland (2007) discusses the major tectonic elements and the regional and local features from outcrops near the margins. Greenland's crust is mostly of Precambrian age and is divided into several major blocks which are briefly described herein, from South to North. The major elements are named Ketilidian, South Greenland Archean, the Nagssugtoqidian, East Greenland Archean, Rinkian, Caledonian Foldbelt, North Greenland, and North Greenland Foldbelt. A map of these geological structures is presented in Fig. 1.

The southernmost Ketilidian mobile belt formed in the Early Proterozoic (ca. 2.1 Ga). The orogeny was likely Andean-style with granodiorite (1.9–1.8 Ga) and anorogenic granite intrusions (1.7 Ga) and equivalent structures in the Makkovik orogeny of Labrador. More recent uplift of the Ketilidian coastal areas is associated with the rifting in the North Atlantic and Labrador Sea. Along the northern boundary, Ketilidian sediments and volcanics were thrust over the Archean basement.

The Archean block north of the Ketilidian block hosts some of the oldest rocks (ca. 3.8 Ga) on Earth. This block probably has the greatest thermal age and therefore the highest rigidity and crustal thickness. Additional thickening resulted from dike intrusions between 2.7 and 1.7 Ga and crustal inflation due to the rifting in the Labrador Sea and the North Atlantic.

Along the northern boundary, the Archean block is thrust over the Nagssugtoqidian mobile belt consisting primarily of reworked Archean rocks and large quantities of Proterozoic gneisses. This belt may also include

a suture where Archean blocks collided during the Early Proterozoic. Crustal thickening intrusions, dike swarms and other igneous features were emplaced at ca. 2.8–2.7 Ga and 2.0–1.3 Ga. Crustal inflation and magmatism related to the presumed passage of the Iceland hotspot including lateral material flow may have further thickened the Nagssugtoqidian crust (Larsen et al., 1999; Nielsen et al., 2002).

Bordering the Nagssugtoqidian on the north, the Proterozoic Rinkian mobile belt was significantly deformed and metamorphosed during the Hudsonian orogeny at ca. 1.8 Ga. The Rinkian and Nagssugtoqidian belts seem quite similar geologically and therefore their boundary is not well defined. The northern boundary, interpreted mainly from magnetic observations (Brozina, 1995), appears to cross the Caledonian Foldbelt at 74°N. The Iceland hotspot presumably passed through the Rinkian at ca. 75–55 Ma (Müller et al., 1993; Lawver and Müller, 1994).

The East Greenland Archean block has been interpreted as part of the Archean crust comparable to the Archean block in the South. However, the boundaries to the Nagssugtoqidian and the Ammassalik mobile belt and its extent to the North are not clear. Early Tertiary volcanism related to the Iceland plume activity has covered the Archean crust with flood basalts.

The East and West Greenland Tertiary basalt provinces were generated at almost the same time but with contrasting styles. The East Greenland Phanerozoic flood basalt provinces range from Kangerdlugssuaq to the Scoresby Sund and are associated with the formation of the Vøring Plateau, Greenland-Faeroer Ridge, and British Tertiary Igneous Province. The onset time and the volume of flood basalts and seaward dipping

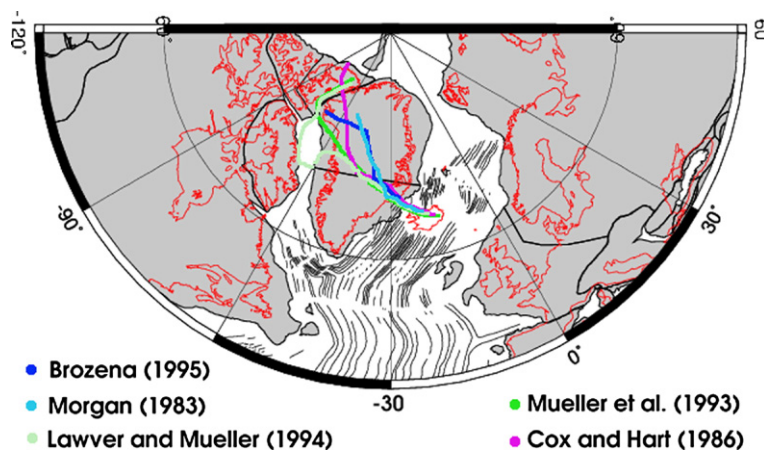


Fig. 3. Iceland hotspot tracks based on five different reconstructions between 150 Ma and present. While the track is well constrained in the last 60 Ma, the reconstructions show significant differences for previous times. Note that some hotspot tracks end prior to 150 Ma.

reflector sequences (Hinz, 1981) suggest the Iceland plume as a likely source. Iceland plume volcanism also affected the non-volcanic extension of the West Greenland margin of the Labrador Sea at ca. 62 Ma with the greatest volcanic activity located at Disco Bay.

East Greenland's crystalline basement consists of gneisses and granitoid rocks with overlying Proterozoic and Palaeozoic sediments. Proterozoic Grenvillian tectonism reworked the basement rocks into a paragneiss complex hosting granite intrusions. The closing of the Iapetus by the collision of Laurentia and Baltica produced the 1300 km long and 300 km wide belt Caledonian Foldbelt along the eastern Greenland margin. Following the orogeny, Devonian extensional faulting formed north–south striking basins with sediments up to 8 km thick. Carboniferous and Mesozoic sedimentary basins also developed before Late Palaeocene block

faulting and rifting initiated the opening of the North Atlantic. The ages of Tertiary alkaline volcanism in the south are ca. 57–47 Ma and much younger in the north, presumably reflecting the development of the Mid-Atlantic ridge northwards from Iceland (Bernstein et al., 1998).

The northern boundary of the Rinkian with North Greenland is also poorly defined. The southern portion of North Greenland belongs to the Greenland shield, whereas in the north the Palaeozoic Franklinian Basin, which extends eastwards from Ellesmere Island to the Wandel Sea, dominates the ice-free areas. In the Mid-to-Late Palaeozoic, the Ellesmerian orogeny cut off sediments to these east–west trending basins. The collision with an unknown continent in the north produced the North Greenland fold belt mostly parallel to the Franklinian basins (Henriksen et al., 2000).

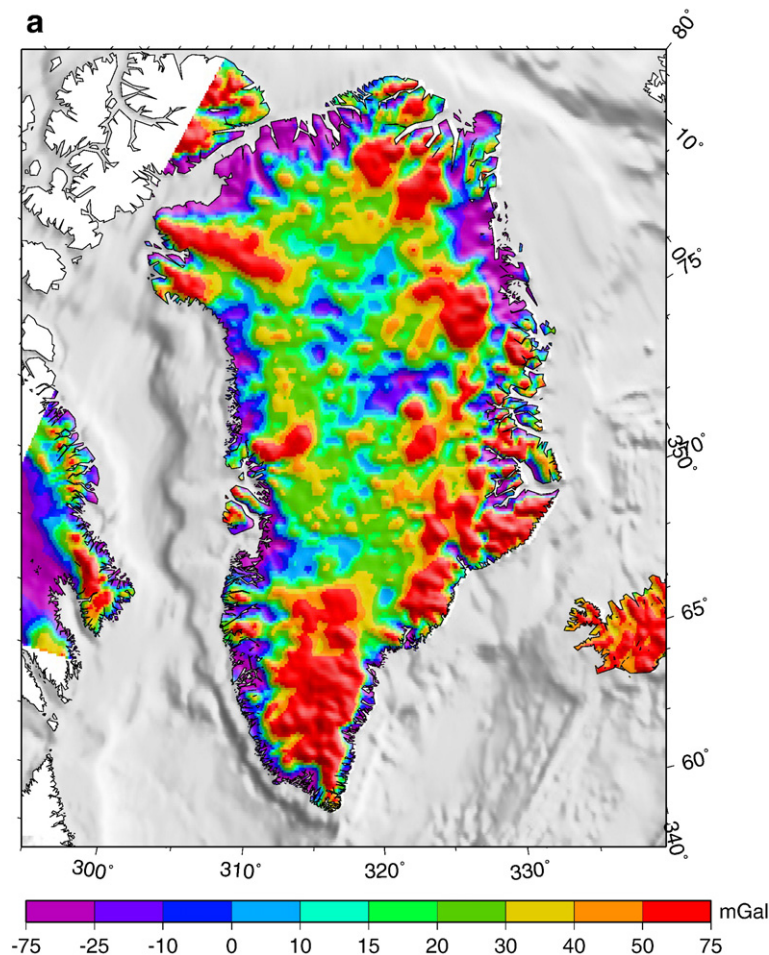


Fig. 4. a: Free-air anomalies from the Arctic Gravity Project (Forsberg and Kenyon, 2003). b: Free-air gravity anomalies upward continued to 20 km altitude.

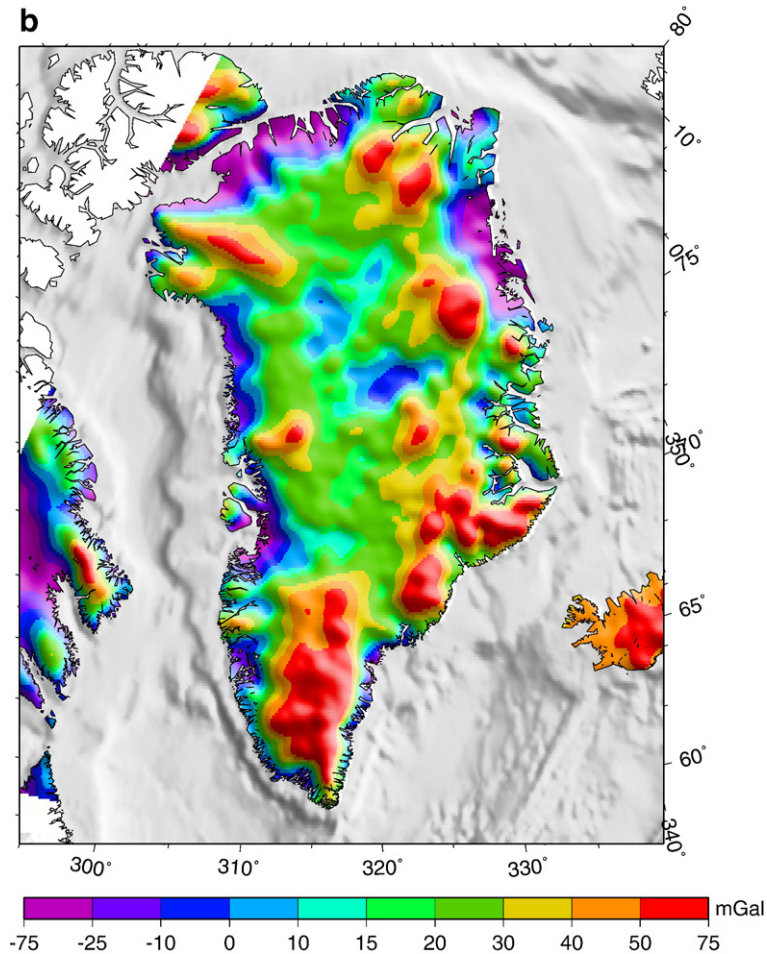


Fig. 4 (continued).

2.2. Plate reconstructions and Iceland hotspot track

In the following, the large-scale tectonic history of Greenland over the last 100 Ma is addressed. During that time period, major events affecting Greenland include sea floor spreading in the Labrador Sea and the North Atlantic, extinction of sea floor spreading in the Labrador Sea, movement of Greenland relative to the Iceland hotspot and several magmatic events in East and West Greenland as well as offshore South Greenland.

Palaeomagnetic data from seafloor basalts allow for the reconstruction of plate motions. Recent studies have shown that hotspots might not be fixed, but moving (Steinberger et al., 2004), although at a rate which is about 1–2 orders of magnitude smaller than the plate motion. Additional information from mantle flow models can assist in such studies to separate the hotspot and

the plate motion. Fig. 2 shows the reconstruction of the North Atlantic between 150 Ma B.P. and present. The reconstruction is based on a fixed hotspot frame after Müller et al. (1993) and plate locations are based on Hay et al. (1999).

Based on different numbers of hotspots and different plate motion data, several hotspot tracks have been proposed and calculated in the past. While the location over the last 60 Ma is in good agreement in most studies, earlier times show significant variations before most hotspot tracks come together in northwest Greenland and Ellesmere Island for times of 120–150 Ma ago.

Paleomagnetic reconstructions of five different sources (Morgan, 1983; Cox and Hart, 1986; Müller et al., 1993; Lawver and Müller, 1994; Brozena, 1995) are shown in Fig. 3. Brozena (1995) suggests a hotspot track channel rather than a track which encompasses

most of the other solutions, with the exception of the track that bends further west into the Labrador Sea (Müller et al., 1993; Lawver and Müller, 1994).

Recent studies of mantle dynamics (e.g. Larsen et al., 1999; Nielsen et al., 2002) have shown that mantle plumes can have a significant component of lateral material flow.



Fig. 5. a: Shaded relief of Greenland by Scambos and Harran (2002) based on the digital elevation model after Ekholm (1996) and enhanced by AVHRR images in the interior ice sheet. b: Bedrock topography of Greenland from the compilation of Bamber et al. (2001). Some areas in central Greenland are below sea level due to the ice loading and related lithospheric deformation.

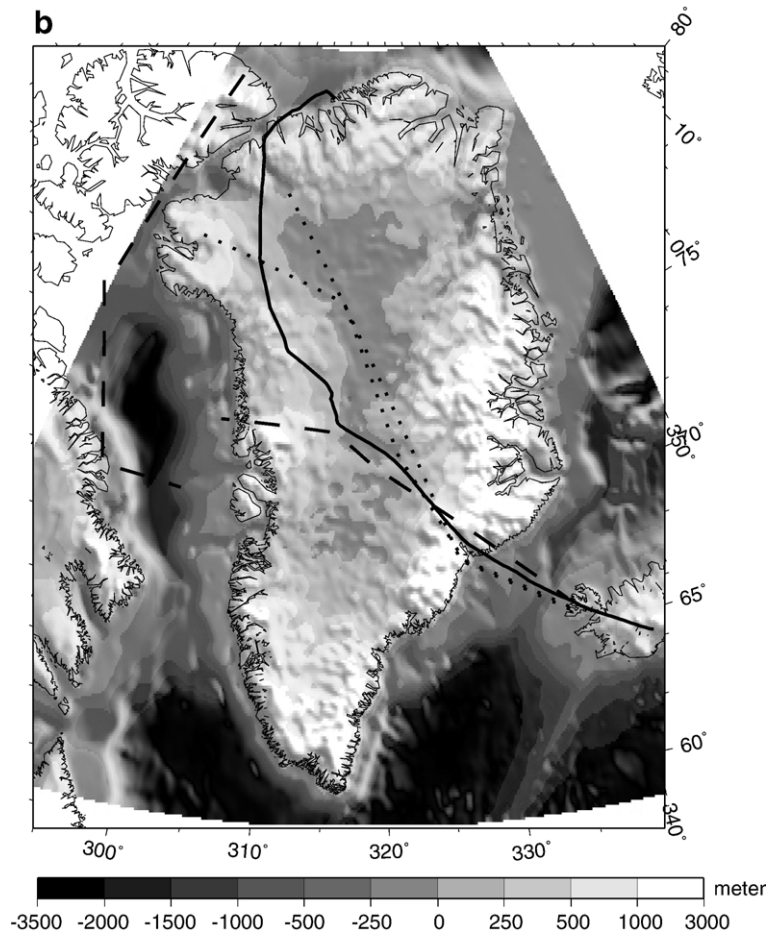


Fig. 5 (continued).

Thermal erosion, lithospheric thinning and other consequences would result from a plume under an old shield such as Greenland.

Unfortunately, the magnetic and sub-ice terrain data of Greenland do not offer much for discriminating between the track estimates because they only marginally constrain the crustal effects of the Iceland hotspot. This is also consistent with the general lack of prominent signatures of the hotspot's effects in the free-air anomalies from the Arctic gravity map (Forsberg and Kenyon, 2003), the surface elevations (Ekholm, 1996) and the bedrock topography (Bamber et al., 2001).

3. Geophysical data

The following geophysical data sets were used in this study: free-air gravity anomalies, bedrock topography, a digital elevation model of the ice sheet, and seismic data

used for Moho depth validation. In addition, seismic tomography, mantle flow and hotspot track models were used to assist in the interpretation.

The recently compiled Arctic gravity map (Forsberg and Kenyon, 2003) and seismic data from the GLATIS project (Dahl-Jensen et al., 2003b) are the major sources of information used to estimate crustal thickness in Greenland. Fig. 4a shows the free-air gravity anomalies in the study area at the Earth's surface that were obtained from the Arctic Gravity Project at the National Imagery and Mapping Agency (NIMA), while in Fig. 4b the upward continued values to 20 km altitude are presented. These free-air gravity anomalies include the results of an extensive aerogravity survey of Greenland by the US Naval Research Laboratory (Brozena, 1995), the Kort & Matrikelstyrelsen (Forsberg and Kenyon, 2003), and shipborne gravity surveys, as well as satellite altimetry-derived anomalies from data sets compiled by NIMA, NASA's Goddard Space Flight Center, and The

Ohio State University (Roman, 1999). The upward continuation applied to the free-air anomalies acts as a low-pass filter which suppresses the small scale gravity variations that are not relevant to the estimation of the crustal thickness (Fig. 4b). The gravity map is dominated by large positive anomalies associated with mountains in South and East Greenland, namely the Archean and Ketilidian blocks in the South, and the Archean and Caledonian Foldbelt in the East (see Fig. 1 for locations).

The Digital Elevation Model (DEM) shown in Fig. 5a is a shaded relief of Scambos and Harran (2002). The DEM is based on the original DEM of Ekholm (1996), with enhancements from Advanced Very High Resolution Radiometer (AVHRR) satellite images (acquired in spring 1997) to improve the spatial detail of the ice sheet surface. The enhanced portion of the relief is limited to the interior region, with a maximum distance of 15 km from the nearest rock outcrops.

The bedrock topography shown in Fig. 5b is based on a compilation of Bamber et al. (2001). The map shows significant depressions in Central Greenland, and at some places, the bedrock is even below sea level. This large-scale depression is associated with the ice load leading to bending of the lithosphere. The deformations caused by changes in ice loading can be separated into two components, an elastic and a viscous component. While the elastic component is mainly caused by recent deglaciation, viscous deformations are mainly due to the deglaciation cycles in the Pleistocene (Tarasov and Peltier, 2002). The elastic response to the known glacial

load provides a means to estimate the “instantaneous” flexural rigidity of the Greenland lithosphere. The current ice load causes the lithosphere to bend by about 700 m in Central Greenland.

The ice thickness, the bedrock topography and the water depth of the surrounding ocean were used to estimate the terrain gravity effect which is required for the crustal thickness estimation.

Additional geophysical constraints on the crustal properties of Greenland are available from magnetic and seismic data. Magnetic anomalies from a compilation of the Geological Survey of Canada (Verhoef et al., 2003) can support the interpretation with respect to the location of the hotspot track and potential volcanic centers. Specifically, the location of the magmatic belt associated with the Iceland hotspot track can be mapped. Seismic tomography data for this area has been published by Bijward and Spakman (1999). The seismic velocity anomalies help to locate large-scale mantle structures. In addition, the mantle flow model of (Steinberger et al., 2004) supports the interpretation and development of a hotspot track scenario.

As was previously mentioned, the gravity and topography data sets were used for modeling and estimating the crustal thickness, while the remaining data sets primarily supported the interpretation.

4. Generalized isostatic modeling of the Greenland crust

In this section, we model the Moho from the gravity effects of the terrain and free-air anomalies at 20-km

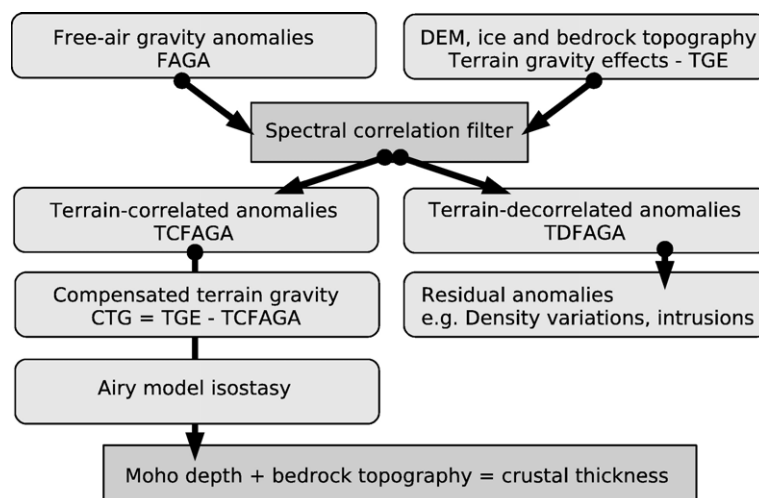


Fig. 6. Scheme of generalized isostatic analysis as used in crustal thickness estimation. Modified after (von Frese et al., 1999).

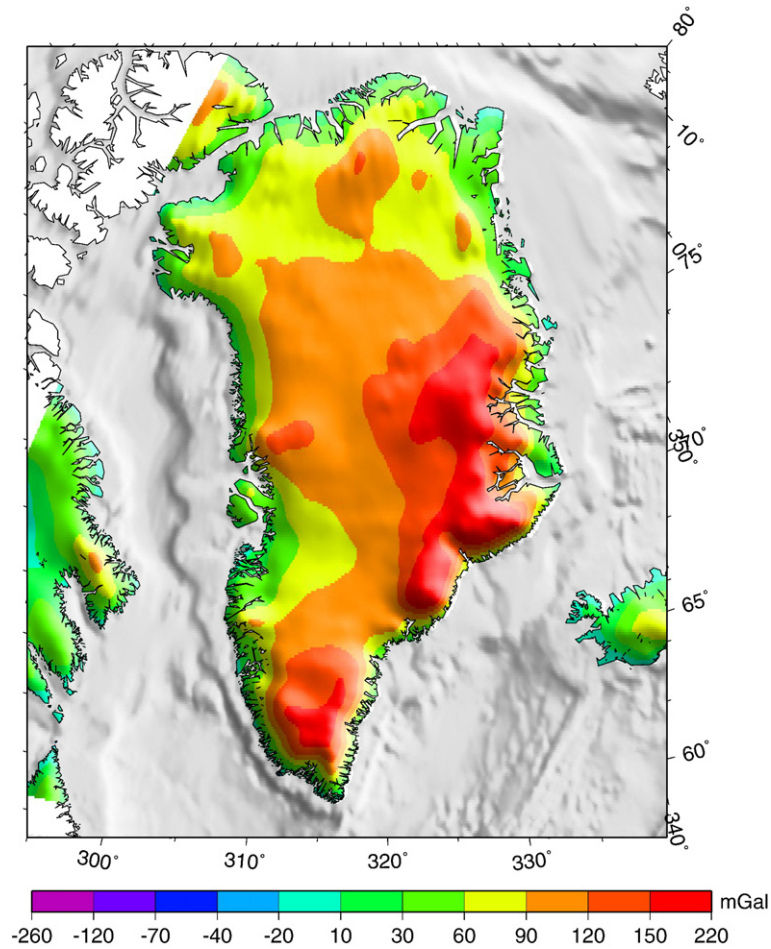


Fig. 7. Terrain gravity effect computed from the ice, water and rock components by Gauss–Legendre quadrature integration (von Frese et al., 1981). Data over ocean shows bathymetry.

altitude for the region (58–84°N, 76–14°W) roughly centered on Greenland.

Fig. 6 presents the scheme which was employed to estimate crustal thickness and Moho depth from gravity and topography data. Further details of the method can be found in (von Frese et al., 1999; Leftwich et al., 2005). The free-air gravity anomalies and the terrain models (bedrock, ice sheet, ocean depth) were correlated to infer the isostatic composition of Greenland's crust.

Fig. 7 gives the integrated gravity effects of the water, ice, and rock components of the terrain (Fig. 5b) modeled in spherical coordinates by Gauss–Legendre quadrature integration (von Frese et al., 1981). These effects were computed using rock, water and ice densities of 2800 kg/m³, 1020 kg/m³, and 900 kg/m³, respectively. Any elevation errors in Fig. 5b and the simplification of using a single density for the

rock component clearly produce local terrain density errors.

However, the 20-km altitude of the analysis, which is large compared to the relief of the terrain, greatly reduces the gravity effects of these errors relative to the regional free-air components defined by the relief of the terrain and the Moho (von Frese et al., 1999; Kim et al., 2000; Potts and von Frese, 2003a; Leftwich et al., 2005).

The free-air anomalies incorporate the gravity effects of all mass variations in the subjacent Earth. The anomalies cannot be separated into their different geological components without additional geological and geophysical constraints. For instance, their correlations with the gravity effects of the terrain will include all isostatic anomalies of the terrain. Hence, the terrain-correlated free-air anomalies can help target isostatically disturbed components of the terrain sustained by lithospheric strength and mantle dynamics.

To evaluate the terrain-correlated free-air components, the correlation spectrum (von Frese et al., 1997) is used between the Fourier transforms F and T of the free-air gravity anomalies at 20-km altitude (Fig. 4b) and the terrain gravity effects (Fig. 7), respectively, given by

$$CC(k) = \cos(\Delta\theta_k) = \text{Re} \left[\frac{\mathbf{F}(k)}{\mathbf{T}(k)} \right] \left[\frac{|\mathbf{T}(k)|}{|\mathbf{F}(k)|} \right]. \quad (1)$$

Here, $CC(k)$ is the correlation coefficient between the k th wavenumber components $\mathbf{F}(k)$ and $\mathbf{T}(k)$ with the amplitude spectra given by $|\mathbf{F}(k)|$ and $|\mathbf{T}(k)|$, respectively, and Re denotes taking the real parts of the wavenumber components. $CC(k)$ is evaluated from the cosine of the phase difference ($\Delta\theta_k$) between the two corresponding k th wavenumber components. The correlation

spectrum only depends on the phase properties between orthogonally gridded and co-registered data sets. Hence, Fourier transforms can be employed to analyze the two data sets in spherical coordinates for their correlations with absolutely no loss of generality.

From the correlation spectrum, spectral filters were developed to extract the terrain-correlated free-air anomalies of the Greenland study region. Specifically, the k -wavenumber components showing positive ($CC_p(k) \geq 0.76$) and negative ($CC_n(k) \leq -0.90$) correlations between the free-air anomalies and the terrain effects were identified. These cutoff values were chosen for the correlation filter to minimize correlative features between the terrain-decorrelated free-air and compensated terrain gravity components so that the two gravity components could be independently analyzed for the properties of the subsurface (e.g. Leftwich et al., 2005). Experience shows

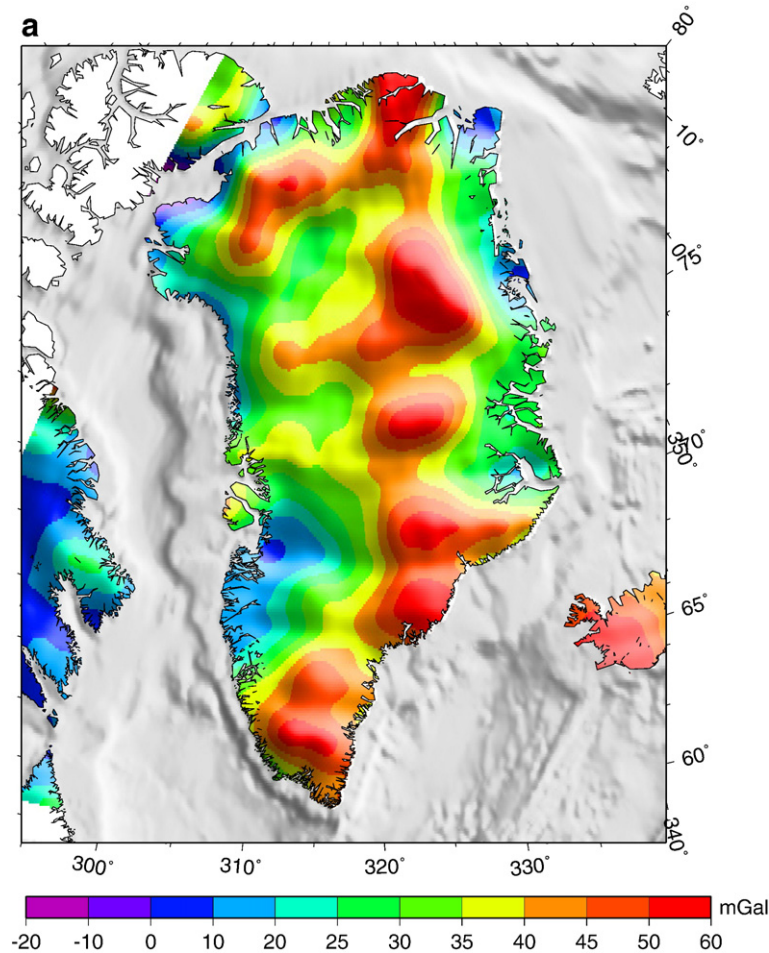


Fig. 8. a: Terrain-correlated anomalies obtained from spectral correlation filtering of upward continued free-air anomalies of Fig. 4b and terrain gravity effects of Fig. 7. b: Terrain-decorrelated anomalies.

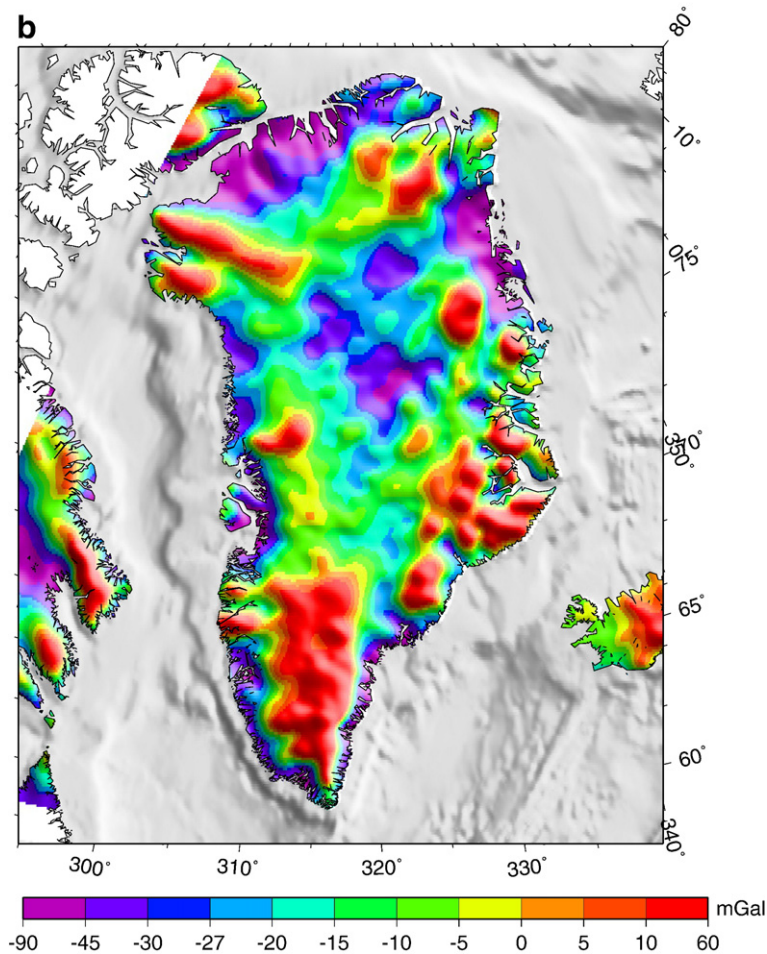


Fig. 8 (continued).

that this selection criterion is relatively robust in establishing an effective starting point for studying how the terrain may relate to the free-air anomalies. The selected cutoff values are not universal, however, and must be assessed in each application for the specific spectral properties that are offered by the related gravity components.

Inversely transforming the correlated free-air wave-number components yields the terrain-correlated free-air anomalies in Fig. 8a, whereas Fig. 8b gives the residual terrain-decorrelated free-air gravity anomalies. The terrain-decorrelated components of the total free-air anomalies in Fig. 8b may well reflect mass variations within the crust and sub-crust (e.g. Potts and von Frese, 2003b). However, the focus of this study is the Moho that accounts for the terrain-correlated components of the free-air anomalies and thus we do not speculate further in this paper on the geological implications of the terrain-decorrelated free-air anomalies.

The more regional terrain-correlated free-air anomalies (Fig. 8a) provide important constraints on crustal structure and dynamics. For example, the zero anomaly marks regions of crustal equilibrium so that positive and negative anomalies will reflect crust in compression and tension, respectively. In other words, positive and negative terrain-correlated free-air anomalies can mark crust that is isostatically too thin (i.e., under-compensated) or thick (i.e., over-compensated), respectively, and hence under pressure to equilibrate by the compressive in-flow or expansive out-flow of crustal material (e.g. Artyushkov, 1973). These anomalies can reflect Moho in uplift or subsidence (e.g., von Frese et al., 1999; Kim et al., 2000), or alternatively dynamic surface topography that is respectively too low or high to be in isostatic equilibrium (Pari, 2001).

In principle, the terrain-correlated free-air anomalies (Fig. 8a) are taken as the terrain isostatic anomalies. It is clear that this interpretation is not unique because terrain-

correlated anomalies may also result from uncompensated mass distributions that are not related to the terrain. However, terrain isostatic effects likely dominate the terrain-correlated free-air anomalies because isostatically disturbed terrain involves the strongest density contrasts of the lithosphere. Thus, subtracting the terrain effects (Fig. 7) from the terrain-correlated free-air anomalies (Fig. 8a) provides estimates of the gravity effects of the compensated terrain. Inversion of these isostatically corrected terrain effects, in turn, models the Moho and related crustal thickness variations.

Fig. 9b gives the Moho estimated from the least squares inversion of the compensated terrain effects assuming that the gravity effects for the density differentials of the crustal thickness variations integrate to zero

at 20-km altitude. Specifically, the Moho was modeled in spherical coordinates using Gauss–Legendre quadrature integration to estimate the tops and bottoms of $0.5^\circ \times 0.2^\circ$ prisms about the reference depth of 25-km below sea level. The mantle density contrast of 400 kg/m^3 relative to the crust was assumed for the prisms across the mean seismic Moho reference depth of the Greenland study region. This density contrast was chosen because inversion tests with geologically viable contrasts ranging from 300 to 600 kg/m^3 found that the affiliated gravity predictions best matched the available seismic Moho estimates (Leftwich et al., 2005).

Fig. 9a shows the related crustal thickness variations obtained by subtracting the Moho estimates in Fig. 9b from the bedrock elevations of Fig. 4b.



Fig. 9. a: Crustal thickness in Greenland obtained from generalized isostatic analysis. The NE Ice Stream (Fahnestock et al., 2001a,c) and major ice core drill sites are marked. Crustal thickness minima correlate with identified sub-glacial melt and fast glaciers. b: Depth to Moho and estimates based on seismic receiver functions (Dahl-Jensen et al., 2003b; ALE; Ramesh et al., 2002) and surface wave dispersion analysis (NOR, ILG; Gregersen et al., 1988). Numbers under the seismic estimates give the seismic minus gravity Moho differences in km.

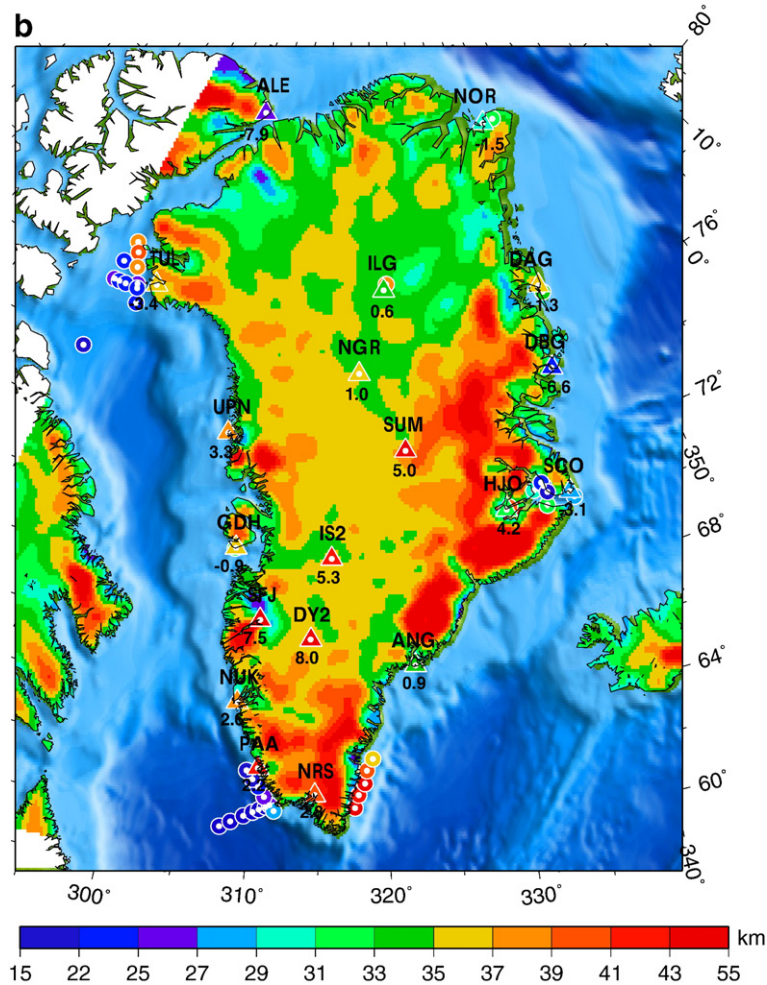


Fig. 9 (continued).

In the next section, the results in Fig. 9 are investigated for extending the very limited outcrop and seismic information that is available on Greenland's crust.

5. Discussion

In this section, we consider the implications of the results of this analysis for augmenting the sparse seismic Moho coverage, and improving our understanding of Greenland's crustal geology including its interaction with the overlying ice sheet and the Iceland hotspot.

5.1. Gravity and seismic Moho estimates

The gravity Moho estimates in Fig. 9b augment seismic Moho estimates from 20 broadband stations on Greenland (Dahl-Jensen et al., 2003b) and about 65 offshore seismic estimates that are concentrated mostly

along the oceanic margins of Greenland and Iceland (Roman, 1999; Leftwich et al., 2005). The seismic Moho does not necessarily coincide with the isostatical Moho as both have different definitions, one reflects the boundary of seismic velocities, the other makes assumptions on the isostatic mechanism, density and temperature. Other sources of seismic Moho depth estimates were obtained from surface wave dispersion analysis (Gregersen et al., 1988).

For continental Greenland and its margin in Fig. 9b, the seismic stations are each marked by a number that indicates in kilometers how much the gravity Moho estimate differs from the seismic Moho estimate. Where the gravity Moho estimate is shallower than the seismic estimate, the number is positive and vice versa. In general, the gravity and seismic Moho estimates match quite well given the commonly reported 2-km error in the seismic measurements (e.g., Dahl-Jensen et al., 2003b).

The greatest misfit is concentrated around 4 broadband stations in central and southern Greenland, where the gravity estimates are 5–10 km shallower. However, adjusting the density contrast for increases up to 1% in the crustal density can force the gravity Moho estimates to match the seismic estimates. Hence, the mismatches are consistent with the occurrence of cold Archean crust in central and southern Greenland where the rocks have somewhat higher densities than those assumed for the analysis. However, these misfits can also reflect seismic errors due to strong converted phases generated at the base of the ice sheet (Dahl-Jensen et al., 2003b) and other uncertainties in recording and processing the seismic data.

Clearly, the gravity Moho and related crustal thickness estimates in Fig. 9 provide new qualitative and quantitative perspectives for extending and testing seismic and other spatially restricted measurements of Greenland's Moho. These measurements, can also be used to test the gravity Moho estimates to help reveal and characterize possible errors in the gravity analysis. Where errors in observations and assumptions are discovered, forward gravity modeling can readily update the gravity Moho estimates.

5.2. Crustal thickness and geology

The average crustal thickness over central Greenland is about 37 km (Fig. 9a), which is in good agreement with crustal thickness values in other cratons and shields (Zandt and Ammon, 1995), e.g. 37 km in Flin-Flon Canada (Zelt and Ellis, 1999), 37–43 km in Brazil (Assumpcao et al., 2002). In general, the gravity crustal thickness data characterize the north Greenland crust as being some 5–10 km thinner than the normal 35–40 km thick crust of the Rinkian and Nagsugtoqidian provinces. On the other hand, crust that is 5–10 km thicker than normal appears to underlie the two Archean provinces and the southern two-thirds of the Caledonian Foldbelt.

The thinner crust of northern Greenland is bifurcated by the N–NE band of thickened crust that appears to connect Proterozoic outcrops of metamorphic gneiss complexes at its northern end (Victoria Fjord) with comparable rocks at its southern end near 76°–77°N on the Melville Bay coastline. The southern margin of the Franklinian Basin in the interior of Greenland is undefined due to permanent ice cover. The basin, however, is clearly part of a substantial region of thinned crust that extends well south of the coastline.

The crustal thickness data also may indicate new constraints on the northern Rinkian boundary, which is

poorly defined under the thick snow and ice cover of central Greenland (Brozena, 1995; Henriksen et al., 2000). At the western end, for example, Fig. 9a suggests the substantial northward extension of normal thickness Rinkian crust. Another northwardly extending lobe is evident at the eastern end that was likely disturbed by the development of the Caledonian Foldbelt.

The Franklinian Basin shows thin crust from the Kane Basin to Peary Land, but the southern extent of the basin is undefined due to permanent ice cover. The crustal thickness map provides an indication of how far south the geological features along the coastline may penetrate the Greenland shield.

The crust is thinner towards the sedimentary basins despite the flat topography, which does not account for the entire large-scale signal. There could be contributions from mantle dynamics that may have led to lithospheric and crustal thinning at times of hotspot activity in this area.

5.3. Crustal thickness and glaciology

In general, thinner crust is warmer than thicker crust by virtue of the enhanced thermal conductivity of the mantle relative to the crust. Furthermore, variations in crustal heat flow may be correlated directly with basal melting, which is a key parameter helping to control the flow of ice sheets (Fahnestock et al., 2001a). Thus, Fig. 9a associates regions of fast glacial ice flow and high basal melt rates with the thinner crust of northern Greenland.

The concentration of Greenland's major active ice streams on the thinned northern crust is clearly consistent with this association. For example, to the northwest, thinned crust underlies the large, fast-moving Petermann and Humboldt Glaciers, whereas the extensive NE Ice Stream overlies the thinned crust of northeastern Greenland. Ice penetrating radar measurements indicate high basal melt rates around the onset of the NE Ice Stream (Fahnestock et al., 2001a), upstream of the NGRIP ice core sites (Dahl-Jensen et al., 2003b), and the Petermann Glacier (Ekholm et al., 1998).

Fig. 9a provides new constraints for modeling crustal heat flow variations that affect basal melting. In general, geothermal heat flux and basal melting (e.g., Blankenship et al., 1993; Huybrechts, 1996; Dahl-Jensen et al., 1997) in combination with the heat flow focusing effects of the sub-ice topography (van der Veen et al., 2007), and the lubricating effects of saturated sediments under the ice (e.g., Bell et al., 1996; Engelhardt and Kamb, 1997; Blankenship et al., 2001; Studinger et al., 2001) are key parameters for understanding ice sheet flow.

Therefore, the crustal thickness results have important implications for mass balance and modeling studies of the Greenland ice sheet.

Basal melt and melt water strongly influence ice flow. The basal temperatures depend on various factors, including the mean surface temperature, the geothermal heat flux, the ice thickness, and the flow pattern. Basal melt under the Greenland Ice Sheet has been derived from modeling studies (Huybrechts, 1996), ice penetration radar profiles (Fahnestock et al., 2001a), and from boreholes reaching the bedrock.

There is growing evidence of extensive basal melt in the central region of northern Greenland. Fahnestock et al. (2001b) determined an age-depth relationship and basal melt rate from ice penetrating radar data in northern Greenland. The study detected high basal melt, in places at rates of up to 0.2 m/yr, under the onset region of the NE Ice Stream and its southern tributaries. This basal melt requires a geothermal heat flux much larger than those typical for old and cold cratonic crust and it could play a major role in initiating the rapid flow of the ice stream (Fahnestock et al., 2001c). The NE Ice Stream, located at the transition zone between the thicker crust of the Rinkian block and the thinner crust of northern Greenland, is distinctly visible on the topography. The onset region of the ice stream is located at the intersection of the lines forming a V-shaped boundary and the ice stream follows the NE–SW boundary of the thin crust of the Northern Greenland block. The observed ice temperature was well above the pressure melting point at the base of the NGRIP deep ice core, drilled on the ice divide 170 km northwest of the onset region of the ice stream (Dahl-Jensen et al., 2003a; Andersen et al., 2004).

The basal melt rate at the base of NGRIP reaches 7.5 mm of ice per year and modeled geothermal heat flow is between 90 and 160 mW/m² along the flow line originating 50 km upstream of the drill site (Dahl-Jensen et al., 2003a). These heat flux values are much higher than those expected over the old craton and their large variance suggests very prominent geological structures under the ice.

An extended study by Fahnestock (personal communication) identified basal melt further north in NE Greenland, in regions draining to Nioghalvfjærdsfjorden and into the Independence Fjord, and in NW Greenland within the drainage basin of Petermann and Humboldt glaciers. The general pattern of basal melt correlates with the thinned crustal thickness estimates with basal melt occurring over the thinnest crust. Model studies (e.g. Huybrechts, 1996) and analysis of surface and bedrock elevations (Ekholm et al., 1998) have suggested that melt occurs upstream of Petermann Glacier, but the new results

by Fahnestock (personal communication) depict a much larger area of basal melt than previously anticipated and shows a strong correlation with the gravity inferred crustal thickness map. The findings of the above studies indicate the importance of basal melt and geothermal heat flux and crustal thickness for the development of the Greenland ice sheet. Excess basal melt water might also contribute to the very high basal melt and explain the mechanism creating under ice furrows under the floating tongue of the Petermann Glacier (Stewart et al., 2004). The estimates presented herein of thinned crust under northern and central Greenland coincide with the areas where higher than expected heat flux and basal melt are detected.

5.4. Crustal thickness and the Iceland hotspot

In this section, we investigate the results of the gravity analysis for constraining the effects of the Iceland hotspot on Greenland's crust. When compared with the estimates in Fig. 9a, none of the projected hotspot tracks appears to show a prominent crustal thickness signature.

However, assuming a plume under an old shield such as Greenland has consequences on the thermal and mechanical properties of the lithosphere. Thermal erosion and both lithospheric thinning and thickening are accepted mechanisms of hotspot–lithosphere interactions (van Wijk et al., 2004; Benoit et al., 2006).

From the variety of different hotspot tracks (Morgan, 1983; Cox and Hart, 1986; Müller et al., 1993; Lawver and Müller, 1994; Brozena, 1995), the most recent solution of Steinberger et al. (2004) is taken as an example. It is based on mantle flow models fitting global hotspots and plate motions. These hotspots are not fixed and can move within the mantle flow, although these motions are rather small compared to the plate motions. This model has led to improved determinations of hotspot tracks in several areas of the world (e.g. O'Neill et al., 2003). The model by (Steinberger et al., 2004) further matches the large-scale mantle structures identified in a seismic tomography model of Bijward and Spakman (1999). A detailed comparison, however, is outside the scope of this study.

In the context of the crustal thickness estimates and other available geological, glaciological, and geophysical data, the following hotspot scenario is proposed for the period 110 Ma to present. At 110–90 Ma BP, the Iceland hotspot was located under the Precambrian block of northwest Greenland. This area does not belong to the Greenland shield and has undergone several deformation events related to the Ellesmere orogeny and the lateral fault zone of the Nares Strait. Magmatic

activity associated with the hotspot may have led to rising mantle material under northwest Greenland leading to initial rifting and a thinned crust. In Fig. 9b, a pronounced minimum at 60°W and 80°N can be identified. Additional indications for unusually high heat flow result from present day basal melting rates of the Petermann Glacier, which is located at the minimum.

While Greenland moved further N–NW, the Greenland shield covered the hotspot, and thick crust blocked the heat flow from penetrating the crust and no clear expression of rifting can be seen both in the gravity data or crustal thickness data. Instead, the material may have expanded laterally to create a broad plume head under northern Greenland.

Thermal erosion may have led to homogeneous crustal thinning, but no rift developed. When Greenland moved further north at 70–56 Ma, the hotspot was located under the Rinkian block, sea-floor spreading in the Labrador Sea was already active and a number of rift axes developed in the North Atlantic as part of the northward-progression of the Mid-Atlantic ridge system.

At about 60 Ma, the hotspot was located at 42°W and 72°N. Ongoing spreading activity in the Labrador Sea and initial rifting in East Greenland at the same time might have interacted with the hotspot activity. It is suggested that both areas might have been fed by mantle material from the hotspot.

Mantle dynamics studies (e.g. Larsen et al., 1999; Nielsen et al., 2002) have shown that mantle plumes can have significant lateral transport of material. Larsen et al. (1999) showed that fast mantle plumes are able to provide the required volume of material to explain the almost simultaneous onset of early Tertiary volcanism in west Greenland and southeast Greenland. Moreover, the lateral flow velocities estimated from their mantle dynamics model can transport magmatic material from the center of the volcanic centers where extensive decompressional melting is forcing the development of volcanic margins.

Nielsen et al. (2002) studied the structure of the West Greenland and Southeast Greenland volcanic margins and suggested a plume model which also includes the interaction with on-going spreading in the Labrador Sea to explain the different spatial dimensions of the volcanic margins. For our study, these findings are important for explaining why the crustal thickness in Southern and Central Greenland is still comparable to cratons not affected by mantle plumes (Zandt and Ammon, 1995; Zelt and Ellis, 1999; Assumpcao et al., 2002). We argue that lateral material flow may have prevented thermal erosion of the crust in these areas and thickening of the crust took place. van Wijk et al. (2004) found crustal

thickening in an extensional regime once the lateral temperature gradient was sufficiently high. In fact, Fig. 9a shows thickened crust underneath the hotspot track along a N–NE striking band between Camp Century and Kangerdlugssuaq. Camp Century potentially marks the transition between thinning and thickening due to hotspot–crust interaction.

About 37 Ma ago, the hotspot was located under the East Greenland shelf, seafloor spreading in the Labrador Sea stopped and the mid-Atlantic ridge system started to reorganize including a jump of the spreading center from the Aegir ridge to the Kolbeinsey ridge (Braun and Marquart, 2004). A part of East Greenland's continental shelf, the Jan-Mayen block, separated from Greenland.

The temporal connection of these events does not seem to be coincidental, and may explain the dramatic change in the plume-lithosphere/crust interaction during the three phases discussed here. It is likely that the lateral flow of mantle material from the hotspot towards the west was stopped by increased activity in East Greenland. Nielsen et al. (2002) support this scenario by incorporating the structure of the West and East Greenland volcanic margins. The increased activity in East Greenland together with the westward motion of Greenland and the opening of the North Atlantic suggest that the volcanic centers in West Greenland (Disco Bay) have been connected to the hotspot as the activity stopped after the hotspot moved further to the east.

Certainly, these scenarios are not exhaustive and their geological validity cannot be determined with only the results and data of this analysis. However, these scenarios predict strongly contrasting styles of hotspot–crust interaction for the N/NE linear crustal thickness band and the adjacent thinned crust of North Greenland. Thus, they might be tested by drilling and dating the intrusions that sample these crustal components.

6. Conclusions

The relationship between Greenland's terrain and free-air gravity anomalies was analyzed for Moho and related crustal thickness estimates to augment the sparse outcrop and seismic information. The gravity Moho variations fit the available seismic estimates with uncertainties of 2–5 km. However, for several broadband stations in central Greenland, the gravity Moho estimates are systematically shallower than the seismic estimates by up to 8 km. These misfits can reflect errors in the gravity and/or seismic data analyses and may be eliminated by adjusting the density contrast model locally for a roughly 1% increase in crustal density. This adjustment would be consistent with local Archean crust that is slightly denser than we had assumed

in the Moho modeling of the isostatically corrected terrain gravity effects.

The crustal thickness estimates indicated an average value of about 37 km for Greenland, with 5–10 km higher values in the southern Greenland Archean blocks and Caledonian Foldbelt, and comparably lower values in northern Greenland. The thinner northern crustal thickness estimates correlated strongly with the faster basal melt regions of the ice sheet and glaciers (Peterman, Humboldt, Kangerdlugssuaq). In addition, a linear N–NE striking band of thickened crust was mapped through north-central Greenland that may relate the crustal geology underneath the ice sheet to outcrops in northern and western Greenland. The Iceland hotspot influenced the development of Greenland's crust and a potential scenario for two different styles of hotspot–crust interactions was proposed. We suggest that initial rifting at the northern margin (100 Ma) was followed by the formation of a broad plume head under the craton of North Greenland (90–70 Ma), before more complex interactions with the Labrador and mid-Atlantic ridge systems took place at about 35–70 Ma. The interaction may be related to crustal thickening along the N–NE striking band in north-central Greenland and the magmatic activities in eastern and western Greenland's Tertiary basalt provinces.

The results of this study are prone to errors and limitations in the data and assumptions by which they were obtained. However, other methods (e.g., seismic) can test our results to help reveal and characterize possible errors in the gravity analysis. Where errors in the observations or assumptions become apparent, straightforward gravity modeling can update the gravity analysis.

Additional perspectives on the crustal and sub-crustal tectonic features of Greenland can result from the newly obtained geopotential field observations of the Oersted and CHAMP magnetic and GRACE gravity satellite missions. The pending GOCE and SWARM satellite missions will soon be providing higher resolution gravity and magnetic gradient measurements, respectively. The satellite observations provide important new boundary conditions to further exploit the geological utility of the regional near-surface geophysical datasets of Greenland considered in this study.

Acknowledgments

The authors thank Rene Forsberg and Steve Kenyon for providing the Arctic Gravity Project data. Comments by two anonymous reviewers greatly improved the manuscript. We also appreciate discussions with John Brozena, Tine Larsen, C.K. Shum and C.J. van der Veen. Funding

for this research was provided by NSERC and GEOIDE NCE (Canada), and the polar programs of NSF and NASA (USA).

References

- Alley, R.B., Gow, A.J., Johnsen, S.J., Kipfstuhl, J., Meese, D.A., Thorsteinsson, T., 1995. Comparison of deep ice cores. *Nature* 373, 393–394.
- Andersen, K.K., et al., 2004. High-resolution record of Northern Hemisphere climate extending into the last interglacial period. *Nature* 431, 147–151.
- Artyushkov, E.V., 1973. Stresses in the lithosphere caused by crustal thickness inhomogeneities. *J. Geophys. Res.* 78, 7675–7708.
- Assumpcao, M., James, D., Snoko, A., 2002. Crustal thickness in SE Brazilian shield by receiver function analysis: implications for isostatic compensation. *J. Geophys. Res.* 107, 101029–101042.
- Bamber, J.L., Payne, Antony J. (Eds.), 2004. *Mass Balance of the Cryosphere — Observations and Modelling of Contemporary and Future Changes*. Cambridge University Press. 662 pp.
- Bamber, J.L., Layberry, R.L., Gogineni, S.P., 2001. A new ice thickness and bedrock data set for the Greenland ice sheet, 1, Measurement, data reduction, and errors. *J. Geophys. Res.* 106 (D24), 33,773–33,780.
- Bell, R.E., Blankenship, D.D., Finn, C.A., Morse, D.L., Scambos, T.A., Brozena, J.M., Hodge, S.M., 1996. Influence of subglacial geology on the onset of a West Antarctic ice stream from aerogeophysical observations. *Nature* 394, 58–62.
- Benoit, M.H., Nyblade, A.A., Pasyanos, M.E., 2006. Crustal thinning between the Ethiopian and East African plateaus from modeling Rayleigh wave dispersion. *Geophys. Res. Lett.* 33, L13301. doi:10.1029/2006GL025687.
- Bernstein, S., Kelemen, P.B., Tegner, C., Kurz, M.D., Blusztajn, J., Kent Brooks, C., 1998. Post-breakup basaltic magmatism along the East Greenland Tertiary rifted margin. *Earth Planet. Sci. Lett.* 160, 845–862.
- Bijward, H., Spakman, W., 1999. Tomographic evidence for a narrow whole mantle plume below Iceland. *Earth Planet. Sci. Lett.* 166, 121–126.
- Blankenship, D.D., Bell, R.E., Hodge, S.M., Brozena, J.M., Behrendt, J.C., Finn, C.A., 1993. Active volcanism beneath the West Antarctic ice sheet and implications for ice-sheet stability. *Nature* 361, 526–529.
- Blankenship, D.D., Morse, D.L., Finn, C.A., Bell, R.E., Peters, M.E., Kempf, S.D., Hodge, S.M., Studinger, M., Behrendt, J.C., Brozena, J.M., 2001. Geological controls on the initiation of rapid basal motion for West Antarctic ice streams: a geophysical perspective including new airborne radar sounding and laser altimetry results. In: Alley, R.B., Bindshadler, R.A. (Eds.), *The West Antarctic Ice Sheet: Behavior and Environment*. American Geophysical Union, pp. 105–121.
- Braun, A., Marquart, G., 2004. Evolution of the Lofoten-Vesterålen margin inferred from gravity and crustal modeling. *J. Geophys. Res.* 109 (B6) 0640410.1029/2004JB003063.
- Bromwich, D.H., Chen, Q.-S., Li, Y., Cullather, R.I., 1999. Precipitation over Greenland and its relation to the North Atlantic Oscillation. *J. Geophys. Res.* 104 (D18), 22,103–22,116.
- Brozena, J.M. *Kinematic GPS and Aerogeophysical Measurement: Gravity, Topography and Magnetism*. PhD Thesis, University of Cambridge, May 1995.
- Cox, A., Hart, R.B., 1986. *Plate Tectonics: How It Works*. Blackwell Scientific Publications, Oxford, UK.

- Dahl-Jensen, D., et al., 1997. A search in north Greenland for a new ice-core drill site. *J. Glaciol.* 43 (144), 300–306.
- Dahl-Jensen, D., Gundestrup, N., Gogineni, S.P., Miller, H., 2003a. Basal melt at NorthGRIP modeled from borehole, ice-core and radio-echo sounder observations. *Ann. Glaciol.* 37, 207–212.
- Dahl-Jensen, T., Larsen, T.B., Woelbern, I., Bach, T., Hanka, W., Kind, R., Gregersen, S., Mosegaard, K., Voss, P., Gudmundsson, O., 2003b. Depth to Moho in Greenland: receiver-function analysis suggests two Proterozoic blocks in Greenland. *Earth Planet. Sci. Lett.* 205, 379–393.
- Ekholm, S., 1996. A full coverage, high-resolution, topographic model of Greenland, computed from a variety of digital elevation data. *J. Geophys. Res.* B10, 21961–21972.
- Ekholm, S., Keller, K., Bamber, J.L., Gogineni, S.P., 1998. Unusual surface morphology from digital elevation models of the Greenland ice sheet. *Geophys. Res. Lett.* 25 (19), 3623–3626.
- Engelhardt, H., Kamb, B., 1997. Basal hydraulic system of a West Antarctic ice stream: constrains from borehole observations. *J. Glaciol.* 43 (144), 207–230.
- Fahnestock, M.A., Abdalati, W., Joughin, I., Brozena, J., Gogineni, P., 2001a. High geothermal heat flow, basal melt, and the origin of rapid ice flow in Central Greenland. *Science* 294, 2338–2342.
- Fahnestock, M.A., Abdalati, W., Luo, S., Gogineni, S., 2001b. Internal layer tracing and age-depth-accumulation relationships for the Northern Greenland Ice Sheet. *J. Geophys. Res.* 106 (D24), 33789–33797.
- Fahnestock, M.A., Joughin, I., Scambos, T.A., Kwok, R., Krabill, W.B., Gogineni, S., 2001c. Ice-stream-related patterns of ice flow in the interior of Northeast Greenland. *J. Geophys. Res.* 106 (D24), 34035–34045.
- Forsberg, R., Kenyon, S., 2003. The Arctic Gravity Project. <http://www.nima.mil/GandG/agg/>.
- Geological Survey of Denmark and Greenland (GEUS), 2007. Geological Map of Greenland. <http://www.geus.dk/geuspape-uk.htm>, last accessed, Jan 25, 2007.
- Gregersen, S., Clausen, C., Dahl-Jensen, T., 1988. Crust and upper mantle structure in Greenland. Recent Seismological Investigations in Europe, Proceedings of the 19th General Assembly of the ESC. Nauka, Moscow, pp. 467–469.
- Hay, W.W., DeConto, R., Wold, C.N., Wilson, K.M., Voigt, S., Schulz, M., Wold-Rosby, A., Dullo, W.-C., Ronov, A.B., Balukhovskiy, A.N., Soeding, E., 1999. Alternative global Cretaceous paleogeography. In: Barrera, E., Johnson, C. (Eds.), *The Evolution of Cretaceous Ocean/Climate Systems*, vol. 332. Geological Society of America, pp. 1–47. Special Paper.
- Henriksen, N., A.K. Higgins, F. Kalsbeek, and T.C.R. Pulvertaft. Greenland from Archaeal to Quaternary. Descriptive text to the Geological Map of Greenland I: 2,500,000. *Geology of Greenland Survey Bull.*, 185:93, 2000.
- Hinz, K., 1981. A hypothesis on terrestrial catastrophes. Wedges of very thick oceanward dipping layers beneath passive continental margins—their origin and paleoenvironment significance. *Geol. Jahrb., Reihe E Geophys.* 22, 3–28.
- Huybrechts, P., 1996. Basal temperature conditions of the Greenland ice sheet during the glacial cycles. *Ann. Glaciol.* 23, 226–236.
- Kim, J.W., von Frese, R.R.B., Kim, H.R., 2000. Crustal modeling from spectrally correlated free-air and terrain gravity data — a case study of Ohio. *Geophysics* 65, 1057–1069.
- Korenaga, J., Holbrook, W.S., Detrick, R.S., Kelemen, P.B., 2001. Gravity anomalies and crustal structure at the southeast Greenland margin. *J. Geophys. Res.* 106 (B5), 8853–8870.
- Larsen, T.B., Yuen, D.A., Storey, M., 1999. Ultrafast mantle plumes and implications for flood basalt volcanism in the Northern Atlantic region. *Tectonophysics* 311 (1–4), 31–43.
- Lawver, L.A., Müller, R.D., 1994. Iceland hotspot track. *Geology* 22, 311–314.
- Layberry, R.L., Bamber, J.L., 2001. A new ice thickness and bed data set for the Greenland ice sheet, 2, relationship between dynamics and basal topography. *J. Geophys. Res.* 106 (D24), 33,781–33,788.
- Leftwich, T.E., von Frese, R.R.B., Kim, H.R., Noltimier, H.C., Potts, L.V., Roman, D.R., Tan, L., 1999. Crustal analysis of Venus from Magellan satellite observations at Atlanta Planitia, Beta Regio, and Thetis Regio. *J. Geophys. Res.* 104, 8441–8462.
- Leftwich, T.E., von Frese, R.R.B., Potts, L.V., Kim, H.R., Roman, D.R., Taylor, P.T., Barton, M., 2005. Crustal modeling of the North Atlantic from spectrally correlated free-air and terrain gravity. *J. Geodyn.* 40, 23–50 (August).
- Morgan, W.J., 1983. Hotspot tracks and the early rifting of the Atlantic. *Tectonophysics* 94, 123–139.
- Müller, R.D., Royer, J.-Y., Lawver, L.A., 1993. Revised plate motions relative to the hotspots from combined Atlantic and Indian Ocean hotspot tracks. *Geology* 21, 275–278.
- Nielsen, T.K., Larsen, H.C., Hopper, J.R., 2002. Contrasting rifted margin styles south of Greenland: implications for mantle plume dynamics. *Earth Planet. Sci. Lett.* 200, 271–286.
- O’Neill, C., Mueller, D., Steinberger, B., 2003. Geodynamic implications of moving Indian Ocean hotspots. *Earth Planet. Sci. Lett.* 215, 151–168. doi:10.1016/S0012-821X(03)00368-6.
- Pari, G., 2001. Crust 5.1-based inference of the Earth’s dynamic surface topography: geodynamic implications. *Geophys. J. Int.* 144, 501–516.
- Potts, L.V., von Frese, R.R.B., 2003a. Comprehensive mass modeling of the Moon from spectrally correlated free-air and terrain gravity data. *J. Geophys. Res.* 108 (E4). doi:10.1029/2000JE001440.
- Potts, L.V., von Frese, R.R.B., 2003b. Crustal attributes of lunar basins from terrain-correlated free-air gravity anomalies. *J. Geophys. Res.* 108, 3-1 (May).
- Potts, L.V., von Frese, R.R.B., Leftwich, T.E., Taylor, P.T., Shum, C.K., Li, R., 2004. Gravity-inferred crustal attributes of visible and buried impact basins on Mars. *J. Geophys. Res.* 109 (E09009). doi:10.1029/2003JE002225.
- Ramesh, D.S., Kind, R., Yuan, X., 2002. Receiver function analysis of the North America crust and upper mantle. *Geophys. J. Int.* 150, 91–108.
- Roman, D.R. An integrated geophysical investigation of Greenland’s tectonic history. PhD Thesis, The Ohio State University, 1999.
- Scambos, T.A., Harran, T., 2002. An image-enhanced DEM of the Greenland ice sheet. *Ann. Glaciol.* 34, 291–298.
- Steinberger, B., Sutherland, R., O’Connell, R.J., 2004. Prediction of Emperor-Hawaii seamount locations from a revised model of plate motion and mantle flow. *Nature* 430, 167–173. doi:10.1038/nature02660.
- Stewart, C., Rignot, E., Steffen, K., Cullen, N., Huff, R., 2004. Basal topography and thinning rates of Petermann Gletscher, northern Greenland, measured by ground-based phase-sensitive radar. Technical Report, vol. 15. FRISP Report.
- Studinger, M., Bell, R.E., Blankenship, D.D., Finn, C.A., Arko, R.A., Morse, D.L., Joughin, I., 2001. Subglacial sediments: a regional geological template for ice flow in West Antarctica. *Geophys. Res. Lett.* 28 (18), 3493–3496.
- Tarasov, L., Peltier, W.R., 2002. Greenland glacial history and local geodynamic consequences. *Geophys. J. Int.* 150, 198–229.
- Thomas, R., Csatho, B., Davis, C., Kim, C., Krabill, W., Manizade, S., McConnell, J., Sonntag, J., 2001. Mass balance of higher-elevation

- parts of the Greenland ice sheet. *J. Geophys. Res.* 106 (D24), 33,707–33,716.
- van der Veen, C.J., Leftwich, T., von Frese, R., Csatho, B.M., Li, J., 2007. Subglacial topography and geothermal heat flux: potential interactions with drainage of the Greenland Ice Sheet. *Geophys. Res. Lett.* 34 (12), L12501. doi:10.1029/2007GL030046.
- van Wijk, J.W., van der Meer, R., Cloetingh, S.A.P.L., 2004. Crustal thickening in an extensional regime: application to the mid-Norwegian Voering margin. *Tectonophysics* 387 (1–4), 217–228.
- Verhoef, J., Roest, R., Macnab, R., Arkani-Hamad, J., 2003. Magnetic Anomalies of the Arctic and North Atlantic Oceans and Adjacent Land Areas. GSC Open Files 3125,3280,3281,3282, NRCan-GSC Atlantic, Natural Resources Canada, GSC, Dartmouth NS, Canada.
- von Frese, R.R.B., Hinze, W.J., Braile, L.W., Luca, A.J., 1981. Spherical earth gravity and magnetic anomaly modeling by Gauss–Legendre quadrature integration. *J. Geophys.* 49, 234–242.
- von Frese, R.R.B., Tan, L., Potts, L.V., Kim, J.W., Merry, C.J., Bossler, J.D., 1997. Lunar crustal analysis of Mare Orientale from topographic and gravity correlations. *J. Geophys. Res.* 102, 25657–25675 (November).
- von Frese, R.R.B., Potts, L.V., Tan, L., Kim, J.W., Leftwich, T.E., Merry, C.J., Bossler, J.D., 1998. Comparative crustal modeling of the Moon and Earth from topographic and gravity correlations. *Lunar Planet. Sci.* (XXIX-CDROM, Abstract 1870).
- von Frese, R.R.B., Tan, L., Kim, J.W., Bentley, C.R., 1999. Antarctic crustal modeling from the spectral correlation of free-air gravity anomalies with the terrain. *J. Geophys. Res.* 104 (B11), 25,275–25,296.
- Wahr, J., van Dam, T., Larson, K., Francis, O., 2001. Geodetic measurements in Greenland and their implications. *J. Geophys. Res.* 106 (B8), 16,567–16,581.
- Zandt, G., Ammon, C.J., 1995. Continental crust composition constrained by measurements of crustal Poisson's ratio. *Nature* 374, 152–154.
- Zelt, B.C., Ellis, R.M., 1999. Teleseismic receiver function analysis in the Trans-Hudson Orogen, Saskatchewan. *Can. J. Earth Sci.* 36, 585–603.